Materialia 15 (2021) 101050

Contents lists available at ScienceDirect

Materialia

journal homepage: www.elsevier.com/locate/mtla

Full Length Article

Mechanical and electronic properties of CeO_2 under uniaxial tensile loading: A DFT study

Zhao Liu [a], Biao Wang [a,*], Claudio Cazorla [b]

[a] Sino-French Institute of Nuclear Engineering and Technology, Sun Yat-sen University, Zhuhai 519082, China
[b] Departament de Física, Universitat Politècnica de Catalunya, Campus Nord B4-B5, Barcelona 08034, Spain

ARTICLE INFO

Keywords:
CeO_2
Mechanical properties
Ideal strength
Band gap
SOFCs
DFT

ABSTRACT

CeO_2 is a promising candidate for materials utilized in solid oxide fuel cells (SOFCs) due to its high ionic conductivity. The high operating temperature of SOFCs results in residual thermal stress in the composing materials. In this work, we studied simultaneously the mechanical and electronic behavior of CeO_2 under different uniaxial tensile loading directions using density functional theory. CeO_2 shows strong anisotropic mechanical and electronic behavior under uniaxial tensile strain that it has the highest ideal strength and fracture strain along [100] direction. Meanwhile, [100] tensile strain also leads to the largest band gap reduction compared with the other two strain directions. The analysis of the mechanism shows that the highest strength along [100] direction is from the highest Young's modulus and surface energy. Meanwhile, the analysis on the band gap variation using a theoretical model previously developed by us suggest that the largest average bond length and dielectric susceptibility variation leads to the largest band gap reduction when [100] tensile strain is applied to CeO_2. Therefore, the current study provides a meaningful insight into the mechanical and electronic properties of CeO_2 under stress, which is vital for its application as SOFCs' materials.

1. Introduction

Solid oxide fuel cell (SOFC) [1] is a conversion device which produces electricity directly from oxidizing a fuel, such as H_2 or CO [2]. It is regarded as one of the most promising energy technologies due to its high power density and wide applications ranging from small auxiliary power units to stationary power plants [3]. In addition, it is advantageous also because of its nonpolluting emissions and low greenhouse gas generation [4]. Despite the geometry (planar and tabular) of a SOFC, there are principally three components, including the porous anode, cathode and the dense electrolyte membrane. The cathode catalyzes the oxygen reduction reaction while the anode catalyzes the fuel oxidation reaction. The electrolyte membrane serves to separate the air and fuel and is ideally a pure oxygen ion conductor [5]. What hinders the commercialization of SOFCs on the large scale is its high operating temperature, usually 500–1000°C [6], which brings problems and demands for the materials used in the cell. For instance, the high temperature requires high chemical and physical stability while the cycling operation leads to residual thermal strain in the composing materials, which may degrade their mechanical and electronic properties such as strength and conductivity [7,8]. Thus, for the reliable application of materials on SOFCs, it is vital to understand their mechanical properties under strain. On the other hand, stress may arise from differential thermal expansions and can significantly alter the electronic properties of strained materials, which may degrade the conductivity of electrolyte or redox activity of the electrodes. In light of this, it is also important to under the electronic properties of materials utilized in SOFCs under strain.

CeO_2 is a rare earth oxide which has cubic fluorite structure giving it enough space for the formation and migration of oxygen vacancy [9]. CeO_2 also possesses good physical and chemical stability with high concentration of oxygen vacancy [10,11]. Besides, the ready redox between Ce^{3+} and Ce^{4+} endows it good catalytic activity [12]. Thus, CeO_2-based materials are proper candidates for utilization either as electrodes or electrolytes because of their high catalytic activity and/or ion conductivity [13–15]. For electrolytes, high ionic conductivity and low electronic conductivity is wanted for the minimum voltage loss while for anodes, good catalytic performance is wanted for the efficient conversion of fuel(s). Researchers have been attempting to understand the modifications on the mechanical and electronic properties of CeO_2 that result from thermal stress [16]. A wide range of experimental and theoretical work have previously been done on CeO_2 for application as SOFC anodes and electrolytes [17,18]. However, it is to our knowledge that no previous paper has investigated both the mechanical and electronic properties of CeO_2 simultaneously under strain.

* Corresponding author.
E-mail address: wangbiao@mail.sysu.edu.cn (B. Wang).

https://doi.org/10.1016/j.mtla.2021.101050
Received 19 January 2021; Accepted 18 February 2021
Available online 23 February 2021

Table 1
Comparison of the elastic constants (C_{11}, C_{12}, C_{44}) and band gap of CeO_2 in this work between the previous experimental and theoretical results. MD stands for molecular dynamics.

	Method	Lattice constant (Å)	C_{11} (GPa)	C_{12} (GPa)	C_{44} (GPa)	Band Gap (eV)
This work	DFT	5.39	359 (PBE)	111 (PBE)	60 (PBE)	3.23 (HSE06)
Ref.	Exp.					2.9-3.4 [23,24]
Ref.	GGA	5.42	354 [25]	101	53.2	
Ref.	LDA+U	5.40	355 [26]	139	51	
Ref.	MD	5.47	450 [27]	102	98	

In this work, we study both the mechanical and electronic behavior of CeO_2 under different uniaxial tensile loading directions by means of density functional theory (DFT). The results suggest that CeO_2 shows strong anisotropy in both the mechanical and electronic properties. Combining Griffith theory with our DFT results successfully explain the anisotropic strength of CeO_2. The anisotropic variation of the band gap is qualitatively explained by a simple theoretical model previously proposed by us [19], which reassures its validity. The findings presented in this work provide meaningful results for application of CeO_2 in SOFCs.

2. Computational methods

First-principles calculations based on density functional theory are performed to simulate the effect of uniaxial tensile strain on CeO_2. We use the PBE functional as is implemented in the VASP software package [20] for calculations of the elastic constants. The electronic structures for electrons are described by projector augmented wave (PAW) method. Wave functions are represented in plane-wave basis truncated at 650 eV. For integrations within the Brillouin zone, we employ Γ-centered k-point grids with a density equivalent to that of 8 × 8 × 8. The geometry relaxations are performed with a conjugate-gradient algorithm. The convergence threshold for electronic self-consistent field (SCF) and forces acting on the atoms are 1×10^{-6} eV and 0.01 eV•Å^{-1}, respectively. To obtain the strain-stress curves, a small uniaxial tensile strain was applied sequentially to the unit cell which is relaxed in the previous step. The stress is defined as the force per deformed area and the strain is defined as the true strain. This method has been proved to be an effective tool to study the intrinsic failure mechanism of materials at the atomic scale [21,22]. The Young's moduli of CeO_2 are calculated by the Voigt-Reuss-Hill method as implemented in VASP.

3. Results and discussion

We calculated the lattice constant, elastic mechanical parameters (C_{11}, C_{12} and C_{44}) and band gap of CeO_2 to validate our methodology. Table 1 lists the comparison between our results and previously reported experimental and theoretical results. It can be seen that all the values calculated in this work are in good accordance with previous results with no large difference between either the first-principles methods or classical methods. In order to accurately reproduce the band gap values, all the band gap results are calculated using HSE06 hybrid functional. The band gap is calculated to be 3.23 eV which matches well with the experimental values considering the band gap of CeO_2 is morphology and/or size dependent properties [17,18]. Therefore, comparison of the mechanical and electronic data of CeO_2 between our results and the literature in Table 1 validate our calculation methodology.

Fig. 1 shows the stress response as a function of applied strain. All the tensile stresses linearly increase with the strain at the initial loading stage and the slope of the [100] curve is the sharpest, suggesting that the modulus along [100] direction is the highest, while the moduli along the other two directions are much lower and are close to each other. This suggests that CeO_2 can resist the largest deformation along [100] uniaxial loading direction, while it is much weaker resisting uniaxial loading along [110] and [111] directions. After the initial stage, the stresses show nonlinear increase with the strain and the slope of the curves gradually decrease, indicating softening of the structure. With further increase of the tensile strain, structural failure occurs and the fractured structures are shown in Fig. 1b. The maximum stress along [100] uniaxial tensile loading is 69.7 GPa, while they are 16.2 and 13.5 GPa for [110] and [111], respectively. Furthermore, the structure failure for [100] happens when the strain reaches 0.47, followed by 0.32 for [110] and 0.22 for [111]. The corresponding mechanical values retrieved from Fig. 1a are listed in Table 2. These data suggest that when CeO2 is subjected to uniaxial tensile loading, the fracture will mostly happen when the loading direction is along [111] direction while [100] displays the highest strength among the three low-index directions.

Table 2
Ideal strengths and fracture strains of CeO_2 under different tensile loading directions.

Direction	[100]	[110]	[111]
Ideal strength (GPa)	69.7	16.2	13.5
Failure strain	0.47	0.32	0.22

In order to explain the anisotropic fracture strength of CeO_2 along different uniaxial tensile loading directions, the well-established Griffith criterion is adopted [28]. According to Griffith theory, the fracture strength of a material is expressed by the following equation,

$$\delta_f = \sqrt{\frac{2\gamma_s Y}{\pi a}} \tag{1}$$

where σ_f is the value of the stress at which fracture occurs, γ_s is the surface energy of newly created surface due to crack propagation, Y is the Young's modulus and a is half of the crack length. So for materials with cracks, this equation indicates that fracture occurs when the incremental release of stored strain energy caused by the increase in crack length becomes larger than the increase in surface energy by creation of new surface area. It should be noted that Eq. (1) can also be used to estimate the ideal strength of a perfect material when a is considered as the lattice constant instead of the crack length.

Fig. 2a shows the structures of the three low-index surfaces of CeO_2. Since (100) slab is a polar surface which has a nonzero dipole moment normal to the surface, to eliminate the dipole surface, half of the O atoms from the bottom layer is removed to the opposing face in a checkerboard style to fulfill the CeO_2 stoichiometry. The surface energy is calculated by the following equation,

$$\gamma_s = \left(E_{surface} - nE_{bulk}\right)/2S \tag{2}$$

where $E_{surface}$ is the energy of one of the low-index CeO_2 slabs with vacuum, E_{bulk} is the energy of bulk CeO_2 unit cell, and S is the corresponding surface area. The surface energies of the (100), (110) and (111) surfaces are calculated to be 1.704, 1.214 and 0.834 J/m^2, respectively, which is consistent with previously reported energy order that (100) > (110) > (111), further suggesting the reliability of our methods. Fig. 2b shows the visualization of Young's modulus of CeO_2 which is realized by an open source program ELATE [29], using the elastic tensor values calculated by VASP. The Young's modulus of CeO_2 along [100], [110] and [111] are 307, 187 and 165 GPa, respectively, which follows same order as the surface energy as [100] > [110] > [111]. Therefore, according

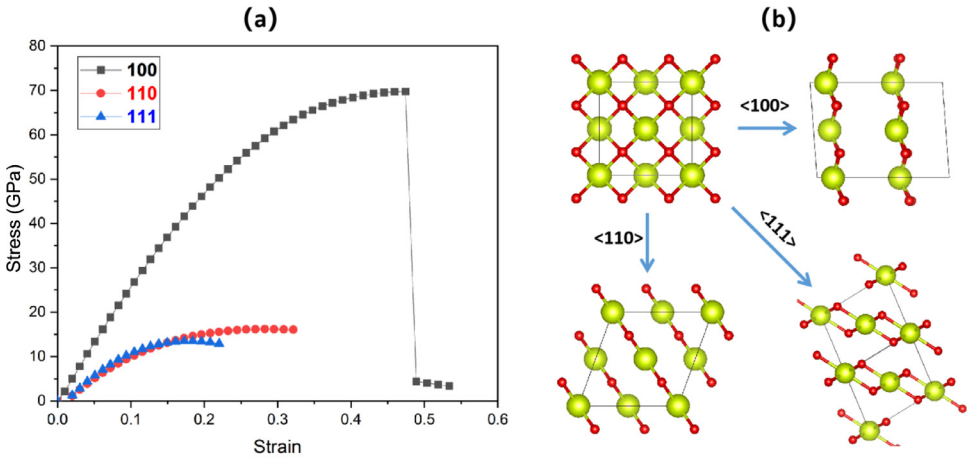

Fig. 1. (a) The calculated stress-strain relations of CeO_2 under different uniaxial tensile loading; (b) The fractured structures of CeO_2 under different uniaxial tensile loading.

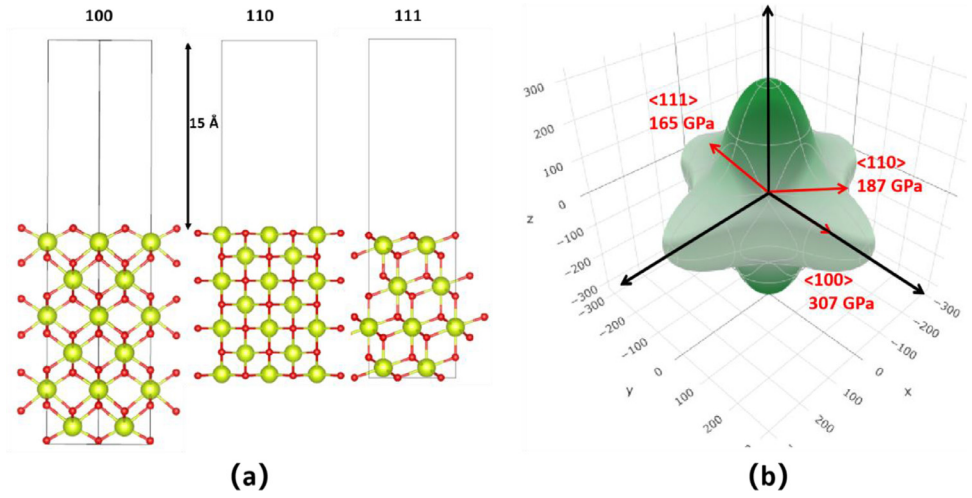

Fig. 2. (a) The structure of the three low-index surfaces of CeO_2; (b) Visualization of Young's modulus of pristine CeO_2 in 3-dimensional.

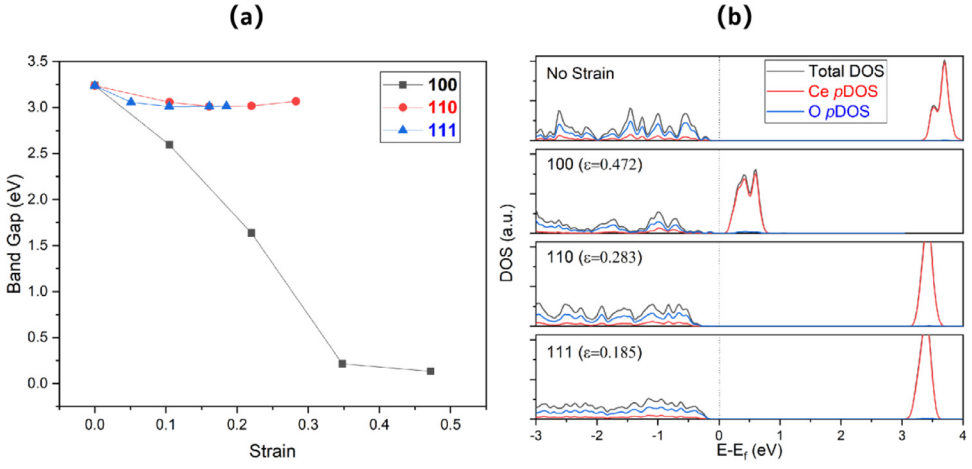

Fig. 3. (a) Band gap changes induced by different uniaxial tensile loading directions; (b) Corresponding partial density of electronic states (*p*DOS) of CeO_2 at the largest strain before fracture.

to Eq.(1), the fracture strengths of CeO_2 along the three uniaxial tensile loading directions have the order of [100] > [110] > [111], which matches exactly with the results in Fig. 1a and Table 2. Thus, the highest strength of CeO_2 along [100] direction is attributed to the highest surface energy and Young's modulus, which demonstrates that the different surface energies and Young's modulus determine the anisotropic mechanical strength of CeO_2 under different uniaxial tensile loading directions.

For application of CeO_2 as either the electrode or electrolyte material in SOFCs, it is important to study its electronic properties under strain. Fig. 3a shows the band gap changes induced by the tensile strain along the three different loading directions and Fig. 3b shows the corresponding DOS and pDOS of the structures at the specific strains. It can be seen that with the increase of uniaxial tensile strain, the band gap of CeO_2 all decrease. The band gap drops tremendously from 3.2 eV to almost zero when CeO_2 is subjected to [100] tensile strain, while the band gap drops slightly to approximately 3 eV for [110] and [111] tensile loading. This suggests that the band gap for CeO_2 is quite sensitive to [100] tensile strain.

Table 3
Relative band gap changes calculated at the ideal tensile strain along different loading directions. $\Delta\chi$ and Δd represent the variation in the dielectric susceptibility and average Ce-O bond length as referred to the unstrained case. [model] refers to the relative band gap variations estimated with the analytical model expressed in Eq. (3), while [DFT] refers to the values obtained directly from the DFT calculations as shown in Fig. 3.

Direction Strain (η)	$\frac{\Delta\chi}{\chi}$	$\frac{\Delta d}{d}$	$\frac{\Delta E_g}{E_g}$ [model]	$\frac{\Delta E_g}{E_g}$ [DFT]
[100] 0.47	15.926	0.710	−867.32%	−95.83%
[110] 0.32	−0.219	0.088	2.20%	−5.25%
[111] 0.22	−0.069	0.054	−1.97%	−6.86

In order to study the mechanism of the band gap variation, we have previously developed a theoretical model that can explain and predict, at a qualitative level, the band gap change of oxides under epitaxial strain [19]. This model is proposed based on well-established solid-state theories that the band gap of a material is related to its crystal field, which in turn is determined by the interatomic distances and dielectric screening. In particular, the analytical model to predict crystal band gap variations as induced by epitaxial strain reads as follows:

$$\frac{\Delta E_g(\eta)}{E_g} = -\frac{1}{2}\left(\frac{\Delta\chi(\eta)}{\chi(0)} + 2\cdot\frac{\Delta d(\eta)}{d(0)}\right) \quad (3)$$

where "0" represents the unstrained case while η represents the epitaxial strain, $\Delta A = \mathrm{A}(\eta) - \mathrm{A}(0)$, d represents the average metal-oxygen bond length. The χ represents the dielectric susceptibility which is calculated by $\chi = \varepsilon_\infty - 1$, where ε_∞ is the ion-clamped dielectric constant of the material. ε_∞ is estimated by the perturbation DFT techniques as implemented in VASP. According to the model, the band gap will decrease along with the decreased atomic distances and/or weakened dielectric screening owing to the decreased crystal filed in the crystal and vice versa. However, it should be noted that the model as expressed in Eq. (3) only provides qualitative prediction since the influence of structural and dielectric factors on the band gap variations are considered independently. The model aims at explaining the mechanism of band gap variations when epitaxial strain is applied, whereas the current study focuses on uniaxial tensile strain. The model is used here to explain the anisotropic electronic behavior of CeO_2 under different uniaxial tensile loading directions thus to verify the validity of the model under a broader scenario (i.e., in the present study η represents uniaxial strain).

Table 3 lists the band gap changes of CeO_2 under different uniaxial tensile loading directions at the largest strain before fracture. The corresponding bond length and charge distribution changes during the process of uniaxial tensile loadings are shown in Supplementary Information. The values for ΔEg/Eg obtained by DFT calculations (Fig. 3) and our analytical model (Eq. (3)) are listed for comparison. For [100] uniaxial tensile strain, there is large increase in the dielectric susceptibility and average Ce-O bond length, therefore, according to the model, the band gap variation is predicted to be ~-860%, suggesting that there would likely to be a band gap closure. This prediction in fact matches quite well with the explicitly calculated DFT results, which show that the band gap of the crystal decreases practically to almost zero (Fig. 3a). As for the cases of [110] and [111] tensile strains, the dielectric susceptibilities decrease slightly while the average bond lengths increase slightly, the band gap variations are calculated to be as small as 2.2% and -1.9%, respectively, which also are in good agreement with the DFT results showing that the η induced band gap variation is below 10%. However, there is a small discrepancy between the model prediction and DFT results for the band gap variation induced by [110] uniaxial tensile strain since the model predicts a slight increase in the band gap while the DFT results show that there is a slight drop. This discrepancy results from the qualitative nature of the model. The analyses presented here elucidate the band gap variation of CeO_2 is from the average bond length and dielectric susceptibility changes during the loading of uniaxial tensile strain. Although the theoretical model shown in Eq. (3) originally was proposed to analyze the influence of epitaxial strain on band gap, the good qualitative agreement between the values predicted by the model and the DFT results in this study suggests the validity of the model under the scenario of uniaxial tensile strain. It is further speculated that the model is valid for broader situations, *i.e.*, if the data of average *ionic* bond length and dielectric susceptibility of an oxide is known, the model can provide qualitative prediction on the band gap variation of materials.

4. Conclusions

In this work, the ideal strength and fracture strength of CeO_2 under three uniaxial tensile loading directions are calculated by means of first-principles methods. It is found that CeO_2 has the highest ideal strength of 69.7 GPa along the [100] direction, while it has the lowest ideal strength of 13.5 GPa along the [111] direction. Griffith theory combined with our DFT results suggest that the strong anisotropic mechanical strength results from the large difference in the surface energy and Young's modulus for the three low-index crystallographic surfaces. Electronic property analyses show significant difference of the band gap reduction among the three tensile loading directions where CeO_2 is quite sensitive to the tensile strain along [100]. The band gap drops to only 0.22 eV when CeO_2 is maximally strained along [100] while the band gap only slightly decreases when maximally strained along the other two directions. An analytical model developed previously by us is used to qualitatively unravel the anisotropic mechanism of the band gap variation. The band gap changes can be explained in terms of the structural and dielectric property variations that alter the crystal field and thus the bonding-antibonding splitting. The present work not only presents the anisotropic mechanical and electronic behaviors of CeO_2 under uniaxial tensile strain but also provides microscopic mechanism that can explain the anisotropy, thus provides meaningful results for applications of CeO_2 in SOFCs and other fields where both mechanical and electronic properties need to be considered. This work also demonstrates that uniaxial tensile loading can be used to tune the electronic properties of CeO_2.

Declaration of Competing Interest

The authors declare that they have no known competing financial interests or personal relationships that could have appeared to influence the work reported in this paper.

Acknowledgments

This work was supported by National Natural Science Foundation of China (12002402, 11832019, 11472313 and 13572355). This work was also supported by the Fundamental Research Funds for the Central Universities (20lgpy186). Z.L. also wants to thank the financial support from the Guangdong overseas young postdoctors recruitment program.

Supplementary materials

Supplementary material associated with this article can be found, in the online version, at doi:10.1016/j.mtla.2021.101050.

References

[1] A.J. Jacobson, Materials for solid oxide fuel cells, Chem. Mater. 22 (3) (2010) 660–674.
[2] L. Fan, et al., Nanomaterials and technologies for low temperature solid oxide fuel cells: recent advances, challenges and opportunities, Nano Energy 45 (2018) 148–176.
[3] S. Hossain, et al., A review on proton conducting electrolytes for clean energy and intermediate temperature-solid oxide fuel cells, Renew. Sustain. Energy Rev. 79 (2017) 750–764.

[4] R.M. Ormerod, Solid oxide fuel cells, Chem. Soc. Rev. 32 (1) (2003) 17–28.
[5] S.C. Singhal, Advances in solid oxide fuel cell technology, Solid State Ion. 135 (1-4) (2000) 305–313.
[6] Y. Zhang, et al., Recent progress on advanced materials for solid-oxide fuel cells operating below 500°C, Adv .Mater 29 (48) (2017) 1700132.
[7] S. Omar, J.C. Nino, Consistency in the chemical expansion of fluorites: a thermal revision of the doped ceria, Acta Mater. 61 (14) (2013) 5406–5413.
[8] H. Masuda, K. Morita, T. Ohmura, Nanoindentation-induced plasticity in cubic zirconia up to 500 C, Acta Mater. 184 (2020) 59–68.
[9] Z. Liu, et al., Growth mechanism of ceria nanorods by precipitation at room temperature and morphology-dependent photocatalytic performance, CrystEngComm 19 (32) (2017) 4766–4776.
[10] C.T. Campbell, C.H. Peden, Oxygen vacancies and catalysis on ceria surfaces, Science 309 (5735) (2005) 713–714.
[11] Hao, X., et al., Atomistic origin of high-concentration Ce3+ in {100}-faceted Cr-substituted CeO2 nanocrystals. Acta Mater. 203: p. 116473.
[12] Z. Liu, et al., Planar-dependent oxygen vacancy concentrations in photocatalytic CeO_2 nanoparticles, CrystEngComm 20 (2) (2018) 204–212.
[13] E. Dogdibegovic, et al., High performance metal-supported solid oxide fuel cells with infiltrated electrodes, J. Power. Source 410 (2019) 91–98.
[14] N.W. Kwak, W. Jung, Analysis of the grain boundary conductivity of singly and doubly doped CeO_2 thin films at elevated temperature, Acta Mater. 108 (2016) 271–278.
[15] K.-W. Park, C.S. Kim, Deformation-induced charge redistribution in Ceria thin film at room temperature, Acta Mater. 191 (2020) 70–80.
[16] A. Selimovic, et al., Steady state and transient thermal stress analysis in planar solid oxide fuel cells, J. Power Source 145 (2) (2005) 463–469.
[17] A. Da Silva, et al., Effect of the type of ceria dopant on the performance of Ni/CeO2 SOFC anode for ethanol internal reforming, Appl. Catal. B Environ. 206 (2017) 626–641.
[18] D. Puente-Martínez, et al., High ionic conductivity in CeO2 SOFC solid electrolytes; effect of Dy doping on their electrical properties, Int. J. Hydrog. Energy 45 (27) (2020) 14062–14070.
[19] Z. Liu, et al., Strain engineering of oxide thin films for photocatalytic applications, Nano Energy 72 (2020) 104732.
[20] G. Kresse, J. Furthmüller, Efficient iterative schemes for ab initio total-energy calculations using a plane-wave basis set, Phys. Rev. B 54 (16) (1996) 11169.
[21] R. Telling, et al., Theoretical strength and cleavage of diamond, Phys. Rev. Lett. 84 (22) (2000) 5160.
[22] D. Roundy, et al., ideal shear strengths of FCC aluminum and copper, Phys. Rev. Lett. 82 (13) (1999) 2713–2716.
[23] Y.-C. Huang, et al., mild synthesis of size-tunable CeO_2 octahedra for band gap variation, Chem. Mater. 32 (6) (2020) 2631–2638.
[24] C. Ho, et al., Morphology-controllable synthesis of mesoporous CeO_2 nano-and microstructures, Chem. Mater. 17 (17) (2005) 4514–4522.
[25] A. Boudjemline, et al., Dependence of pressure on elastic, electronic and optical properties of CeO_2 and ThO_2: a first principles study, Comput. Mater. Sci. 50 (7) (2011) 2280–2286.
[26] S. Shi, et al., First-principles investigation of the bonding, optical and lattice dynamical properties of CeO_2, J. Power Source 194 (2) (2009) 830–834.
[27] Z. Cui, Y. Sun, J. Qu, Molecular dynamics simulation of reduced CeO2, Solid State Ion. 226 (2012) 24–29.
[28] A.A. Griffith, The phenomena of rupture and flow in solids., Philos. Trans. R. Soc. Lond. Ser. A Contain. Pap. Math. Phys. Character 221 (582-593) (1921) 163–198.
[29] R. Gaillac, P. Pullumbi, F.-X. Coudert, ELATE: an open-source online application for analysis and visualization of elastic tensors, J. Phys. Condens. Matter 28 (27) (2016) 275201.